CHEMISTRY
A EUROPEAN JOURNAL

DOI: 10.1002/chem.200800557

Structure, Magnetic Properties, Polarized Neutron Diffraction, and Theoretical Study of a Copper(II) Cubane

Christophe Aronica,[a] Yurii Chumakov,[a] Erwann Jeanneau,[a] Dominique Luneau,*[a] Petr Neugebauer,[b] Anne-Laure Barra,*[b] Béatrice Gillon,*[c] Antoine Goujon,[c] Alain Cousson,[c] Javier Tercero,[d] and Eliseo Ruiz*[d]

Abstract: The paper reports the synthesis, X-ray and neutron diffraction crystal structures, magnetic properties, high field–high frequency EPR (HF-EPR), spin density and theoretical description of the tetranuclear Cu^{II} complex $[Cu_4L_4]$ with cubane-like structure (LH_2 = 1,1,1-trifluoro-7-hydroxy-4-methyl-5-aza-hept-3-en-2-one). The simulation of the magnetic behavior gives a predominant ferromagnetic interaction J_1 ($+30.5\ cm^{-1}$) and a weak antiferromagnetic interaction J_2 ($-5.5\ cm^{-1}$), which correspond to short and long Cu–Cu distances, respectively, as evidence from the crystal structure ($\mathscr{H} = -\sum_{i>j} 2J_{ij}\hat{S}_i\hat{S}_j$). It is in agreement with DFT calculations and with the saturation magnetization value of an S = 2 ground spin state. HF-EPR measurements at low temperatures (5 to 30 K) provide evidence for a negative axial zero-field splitting parameter D ($-0.25 \pm 0.01\ cm^{-1}$) plus a small rhombic term E ($0.025 \pm 0.001\ cm^{-1}$, E/D = 0.1). The experimental spin distribution from polarized neutron diffraction is mainly located in the basal plane of the Cu^{II} ion with a distortion of yz-type for one Cu^{II} ion. Delocalization on the ligand (L) is observed but to a smaller extent than expected from DFT calculations.

Keywords: copper · density functional calculations · EPR spectroscopy · magnetic properties · neutron diffraction

Introduction

As part of many polynuclear frameworks, cubane-like compounds have received considerable attention over the years.[1–13] In the frame of our investigation of polynuclear systems exhibiting magnetic properties we recently reported the synthesis, structure and magnetic properties of two series of heterobimetallic copper(II)–lanthanide(III) compounds with four $[LnCu_3]$ and nine $[Ln_3Cu_6]$ nuclearities based on cubane-like architectures.[14,15]

The chemical approach was based on the use of a simple ligand (LH_2, see below) of the type known to favor cubane-like frameworks. As expected, the reaction gave a tetranuclear complex $[Cu_4L_4]$, abbreviated to $[Cu_4]$, with copper(II) in a cubane-like architecture. The two series of heterobimetallic Ln^{III}–Cu^{II} clusters $[LnCu_3]$ and $[Ln_3Cu_6]$ were then built

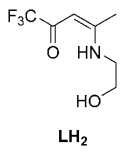

LH_2

[a] Dr. C. Aronica, Dr. Y. Chumakov, Dr. E. Jeanneau, Prof. D. Luneau
Université Claude Bernard Lyon 1
Laboratoire des Multimatériaux et Interfaces (UMR 5615)
Campus de La Doua, 69622 Villeurbanne Cedex (France)
Fax: (+33) 472-431-160
E-mail: luneau@univ-lyon1.fr

[b] P. Neugebauer, Dr. A.-L. Barra
Grenoble High Magnetic Field Laboratory, CNRS
25 Avenue des Martyrs, BP 166
38042 Grenoble Cedex 9 (France)
Fax: (+33) 476-881-111
E-mail: anne-laure.barra@grenoble.cnrs.fr

[c] Dr. B. Gillon, Dr. A. Goujon, Dr. A. Cousson
Laboratoire Léon Brillouin, CEA-CNRS, UMR0012
Centre d'Etudes Nucléaires, Saclay
91191 Gif sur Yvette (France)
Fax: (+33) 169-088-261
E-mail: beatrice.gillon@cea.fr

[d] Dr. J. Tercero, Dr. E. Ruiz
Departament de Química Inorgànica
and Institut de Recerca de Química Teòrica i Computacional
Universitat de Barcelona, Diagonal 647
08028 Barcelona (Spain)
Fax: (+34) 934-907-725
E-mail: eliseo.ruiz@qi.ub.es

Supporting information for this article is available on the WWW under http://dx.doi.org/10.1002/chem.200800557: Selected inter-atomic distances and angles from X-ray diffraction (Table S1). Magnetization at 2 K (Figure S1). Section of the reconstructed experimental spin density in the various Cu–Cu dinuclear planes (Figures S2–S3).

when replacing one or two copper(II) ions of the [Cu_4] cubane core by lanthanide(III) ions (Figure 1).[14]

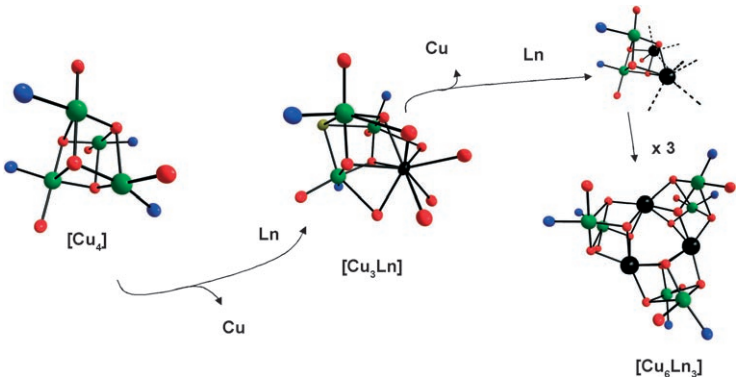

Figure 1. Schematic drawing of the synthesis approach.

Our major concern following this work is to understand the effects on the magnetic behavior when introducing one or several lanthanide ions in copper(II)–lanthanide(III) clusters.[14] Our study raised several interesting questions regarding the magnetic behavior of 3d–4f heterometallic systems. For instance a small anisotropy was revealed for [Gd_3Cu_6][14] while a single-molecule magnet behavior with a strong coercive field was evidenced for [Dy_3Cu_6].[15] In the latter case, the comparison with a previously reported [Dy_3][16] system which possesses a similar {Dy_3} framework but a quasi-null ground spin state seems to indicate that in our system the non-zero ground spin state was favored by the additional copper(II) ion suggestively through spin-frustration effects.

In connection with this approach and to better understand the origin of the magnetism we are now combining high field–high frequency EPR, neutron spin density determination and theoretical studies in the investigation of these systems. HF-EPR measurements should give information on the sign and magnitude of the anisotropy[17] while the polarized neutron diffraction has proven to be relevant to obtain information on the spin delocalization.[18–23] We also performed theoretical studies of the magnetic exchange coupling as well as spin-density calculations using the density functional theory (DFT) formalism. Hence, recently some of us have studied the magnetism of several tetranuclear Cu^{II} complexes (Cu_4) with cubane-like structures. According to the number of short and long Cu–Cu distances, the systems were classified in three different structural types (Figure 2) and theoretical methods based on DFT were used to quantify the strength of the Cu^{II}–Cu^{II} magnetic interactions.[8,12]

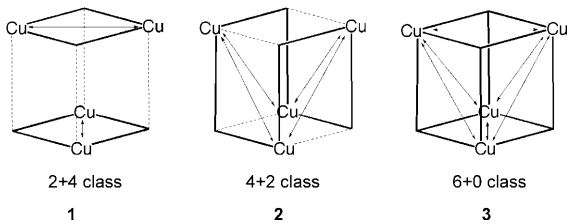

Figure 2. Schematic drawing of the three structural types observed in cubane-like tetranuclear Cu^{II} complexes. Bold and dotted lines stand for short and long Cu–O bond lengths, respectively.

We now present detailed results of our study, combining HF-EPR, neutron spin density determination and a theoretical study of Cu^{II}–cubane [Cu_4].

Results and Discussion

Description of the X-ray structure at room temperature: The crystal structure was described in our previous paper[14] and we briefly summarize the main features. The crystallographic data and refinement details are given in Table 1. Selected bond lengths and angles are given in Table 2 (neutron) and Table S1 (Supporting Information, X-ray).

Table 1. Crystal data and structure refinement for [Cu_4].

Crystal data		
formula	$C_{28}H_{32}Cu_4F_{12}N_4O_8$	
formula weight	1034.74	
crystal system	monoclinic	
space group	$P2_1/c$ (no. 14)	
color	blue	
Z	4	
	Data collections and refinement details	
	X-rays	Neutrons
T [K]	293	30
a [Å]	13.8390(4)	13.393(3)
b [Å]	12.2627(4)	12.207(3)
c [Å]	22.6302(5)	22.82(14)
β [°]	96.785 (2)	97.224(6)
V [Å^3]	3813.5 (2)	3701(1)
ρ_{calcd} [g cm^{-3}]	1.802	1.857
GOF on F^2	1.10	1.011
N reflections used	3573	3958
$R(F)$[a]	0.045 [$I>3\sigma(I)$]	0.0671 [$I>3\sigma(F_o)$]
$R_w(F)$[b] all data	0.056	0.1770

[a] $R(F)=\Sigma\,||F_o|-|F_c||/\Sigma\ \ |F_o|$, [b] $R_w(F)=[\Sigma w(|F_o|-|F_c|)^2/\Sigma w|F_o|^2]^{1/2}$ in which $w=1/\sigma^2$.

The structure is very similar to the one reported with the non-fluorinated ligand.[2] It is made of discrete neutral [Cu_4L_4] molecules (Figure 3) with four Cu^{II} ions and four ligands fully deprotonated (L^{2-}) (see below). The four alkoxo oxygen atoms bridge the copper(II) ions to afford a slightly distorted cubic core {Cu_4O_4}. The copper ions are pentacoordinated with a square base pyramidal environment. The basal plane comprises one nitrogen and two oxygen atoms from one ligand and a third oxygen atom coming from another ligand. The apical position is occupied by an oxygen atom from a third ligand. The Cu–O and Cu–N bond lengths in the O_3N_1 square plane range from 1.890(5) to 1.962(4) Å (average: 1.935 Å) and from 1.930(5) to 1.948(6) Å (average: 1.937 Å), respectively. As it is usually observed, the apical oxygen atom shows a longer Cu–O bond length comprised between 2.400(4) and 2.451(4) Å

Table 2. Selected interatomic distances [Å] and angles [°] for [Cu_4] from neutron diffraction at 30 K.

Cu1–O1	1.886(8)	Cu3–O5	1.921(8)
Cu1–O2	1.996(8)	Cu3–O4	1.962(8)
Cu1–N1	1.923(6)	Cu3–N3	1.958(6)
Cu1–O6	1.992(9)	Cu3–O6	1.971(8)
Cu1–O4	2.409(8)	Cu3–O8	2.461(8)
Cu2–O3	1.949(8)	Cu4–O8	1.954(9)
Cu2–O4	1.978(8)	Cu4–O7	1.967(9)
Cu2–N2	1.946(7)	Cu4–N4	1.947(7)
Cu2–O8	1.976(9)	Cu4–O2	1.928(9)
Cu2–O2	2.338(9)	Cu4–O6	2.466(9)
Cu1···Cu3	3.123(6)	Cu1···Cu2	3.334(7)
Cu1···Cu4	3.152(7)	Cu2···Cu4	3.108(7)
Cu2···Cu3	3.161(7)	Cu3···Cu4	3.298(7)
Cu1-O4-Cu2	98.5(3)	Cu2-O2-Cu1	100.3(3)
Cu2-O8-Cu4	104.5 (4)	Cu4-O8-Cu3	96.0(3)
Cu2-O8-Cu3	90.2 (3)	Cu2-O4-Cu3	106.7(4)
Cu4-O6-Cu3	95.4(3)	Cu3-O4-Cu1	90.6(3)
Cu3-O6-Cu1	104.0(4)	Cu4-O2-Cu2	93.0(3)
Cu4-O6-Cu1	89.4(3)	Cu1-O2-Cu4	106.9(4)

(average: 2.420 Å). The [Cu_4] cluster belongs to the 4+2 class (Figure 2).[12] Four {Cu_2O_2} faces exhibit two different Cu-O-Cu angles (90 and 107°) with three short Cu–O distances (1.96 Å) and a longer one (2.42 Å). In contrast, the two other {Cu_2O_2} faces have similar Cu-O-Cu angles (≈97°) with two short (≈1.96 Å) and two long (≈2.42 Å) Cu–O distances.

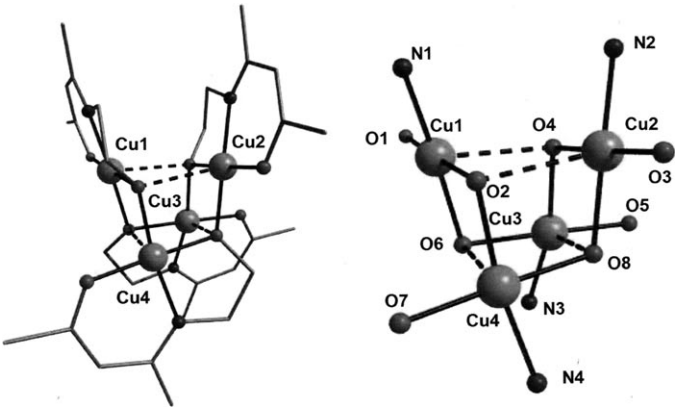

Figure 3. a) Molecular structure of [Cu_4L_4] (L=1,1,1-trifluoro-7-hydroxy-4-methyl-5-aza-hept-4-en-2-one). b) View of the cubane core with labels used in the text.

Description of the nuclear structure at 30 K: The cell parameters refined at 30 K show a shortening of the *a* and *c* cell parameters but the *b* parameter remains similar in the limit of the error bar (Table 1). The interatomic distances and valence angles (Table 2) are very close to those found from the X-ray study (Table S1).

Magnetic behavior: The thermal variation of χT is shown in Figure 4. At room temperature, the χT product of 2.02 $cm^3 K mol^{-1}$ is higher than the expected value for four Cu^{II} ions when considering a *g* value of 2.0 (1.5 $cm^3 K mol^{-1}$). Upon cooling, χT continuously increases and reaches a maximum of 3.55 $cm^3 K mol^{-1}$ at 10 K close to the expected value for an S=2 state. This feature indicates dominant ferromagnetic interactions within the cluster while the χT decrease below 10 K is ascribed to weak intermolecular antiferromagnetic interactions. The magnetization curve recorded at 2 K reaches the saturation value of 4.0 μ_B in agreement with an S=2 ground spin-state (Figure S1, Supporting Information).[14]

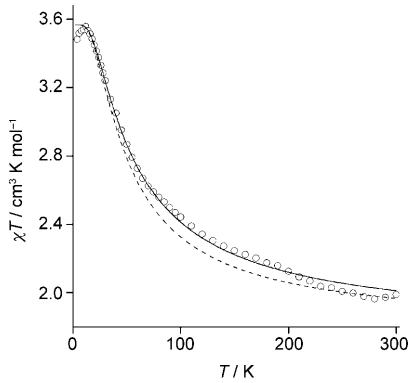

Figure 4. Temperature dependence of the χT product for [Cu_4]. The open circles correspond to the experimental points.[14] The best fit curve is represented by the solid line while that obtained from the calculated *J* values is indicated as a dashed line.

According to the structure and in agreement with the 4+2 class of cubane clusters[12] the data were simulated considering two different coupling constants J_1 and J_2 using the spin Hamiltonian below in Equation (1):

$$\mathcal{H} = -2J_1(\hat{S}_{Cu1}\hat{S}_{Cu4} + \hat{S}_{Cu1}\hat{S}_{Cu3} + \hat{S}_{Cu2}\hat{S}_{Cu4} + \hat{S}_{Cu2}\hat{S}_{Cu3}) - 2J_2(\hat{S}_{Cu1}\hat{S}_{Cu2} + \hat{S}_{Cu3}\hat{S}_{Cu4}) \quad (1)$$

An inter-cluster interaction θ was also included as a mean field correction. The fit procedure leads to the following parameters: $g=2.18$, $J_1=+30.5\ cm^{-1}$, $J_2=-5.5\ cm^{-1}$ and $\theta=-0.10$ K (Figure 4).

EPR Investigations: HF-EPR measurements were performed on a polycrystalline powder sample pressed into a pellet. Spectra were recorded at 190 and 285 GHz at temperatures ranging from 5 to 30 K. In this temperature range, only the S=2 ground spin state is thermally populated (the first excited spin multiplet being about 50 cm^{-1} higher in energy) so that the HF-EPR study allows determining precisely the magnetic anisotropy of this ground state. At 30 K, most of the intensity is found at 9.7 T for an exciting frequency of 285 GHz (corresponding to a $g=2.0$ signal at 10.2 T), which should then correspond to the centre of the spectrum (Figure 5). Conversely at 5 K, the transitions associated to the lowest M_S level ($M_S=-2$) are amplified by the Boltzmann effect and appear at the extremes of the spectrum (at 9.1 and 10.1 T for 285 GHz and 5 K).

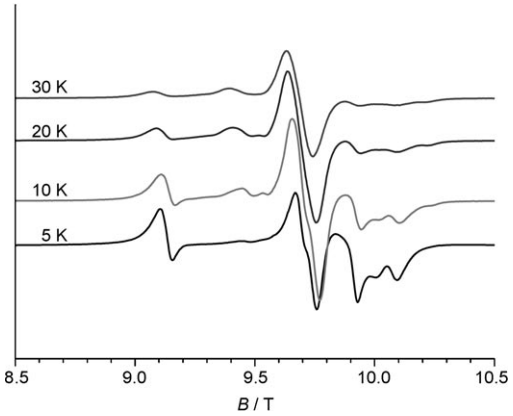

Figure 5. Experimental powder EPR spectra for [Cu_4] recorded on a pellet sample at 285 GHz.

As the low field signal is the farthest from the centre of the spectrum, it corresponds to the $M_S=-2\rightarrow M_S=-1$ transition along the z axis [Eq. (2)] and the zero-field splitting axial parameter D is negative. The set of spectra recorded at both frequencies and for all the temperatures have been calculated by exact diagonalization of the spin Hamiltonian:

$$\mathscr{H} = \mu_B \mathbf{S}\cdot\mathbf{g}\cdot\mathbf{B}+D(S_z^2-S(S+1)/3)+E(S_x^2-S_y^2) \qquad (2)$$

A good agreement with the experimental data has been obtained for the following set of parameters: $D=-0.25\pm 0.01$ cm^{-1}, $E=0.025\pm0.001$ cm^{-1} ($E/D=0.1$), $g_z=2.06\pm0.01$ and $g_x = g_y = 2.115\pm0.005$ (Figure 6).

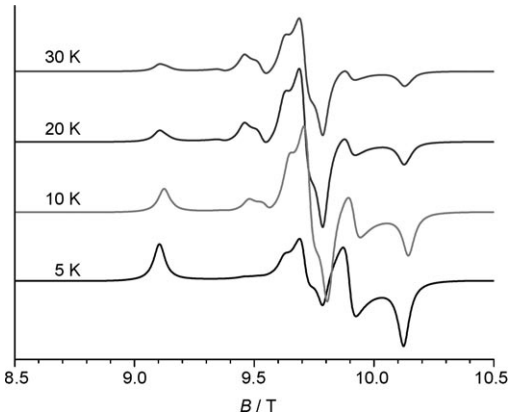

Figure 6. Calculated spectra at 285 GHz with the set of parameters indicated in the text.

The calculation of the dipolar contribution to the zero-field splitting of the $S=2$ ground state, within the point dipole approximation and considering typical g values for Cu^{II} in square pyramidal geometry ($g_{\parallel}=2.34$ and $g_{\perp}=2.08$) is unable to account for the measured values. It leads to a D value about ten times smaller than the experimental one and with the wrong sign (positive D). It indicates that anisotropic exchange contributions to the zero-field splitting should be dominant.[24]

Spin-density reconstruction: We used the so-called Hansen–Coppens model, adapted to spin density,[25] to reconstruct the spin density from the experimental magnetic structure factors. The spin density is written as a sum of atomic spin densities which are developed over the basis of multipolar functions centered on atom i:

$$\rho_i(\vec{r}_i) = \sum_{l=0}^{l=4}\sum_{m=-l}^{l} P^i_{lm} R^i_l(\zeta^i_l,\kappa_i r_i) y^i_{lm}(\theta,\varphi) \qquad (3)$$

where P_{lm} is the population of the multipole lm, R is a Slater-type radial function with exponent ζ and a contraction coefficient κ and y_{lm} is a real spherical harmonics.

We first applied a spherical model for all Cu atoms and their first neighbors:

$$\rho_i(\vec{r}_i) = P^i_{00} N^i_0 r^{n_0 i} e^{-\zeta^i_0 \kappa_i r_i} \qquad (4)$$

The radial coefficients, taken from literature[26] were the following: for Cu, $n_0=4$ and $\zeta=8.8$ u.a.$^{-1}$, for N: $n_0=2$ and $\zeta=3.83$ u.a.$^{-1}$ and for O: $n_0=2$ and $\zeta=4.45$ u.a.$^{-1}$.

The monopole populations were refined as well as the radial exponent of copper (a same contraction coefficient κ was assumed for the four Cu atoms) on the basis of 152 unique reflections with $F_M>3\sigma(F_M)$. An agreement factor $R_w(F_M)=8.47$ and a goodness of fit GOF$=2.54$ were obtained.

In order to determine the nature of the copper 3d orbitals involved in the magnetic interactions, we used a model for the atomic spin density on the copper atoms allowing for the refinement of the five orbital coefficients of the 3d orbital carrying the unpaired electron.[27]

$$\psi_{Cu} = a_1 d_{z^2} + a_2 d_{xz} + a_3 d_{yz} + a_4 d_{x^2-y^2} + a_5 d_{xy} \qquad (5)$$

In this model, the copper atomic density is written as

$$\rho_{Cu}(\vec{r}) = p_{Cu}|\psi_{Cu}(\vec{r})|^2 = p_{Cu}|\sum_{M=-2}^{2} a_{2M}\phi_{2M}(\vec{r})|^2 \qquad (6)$$

where p_{Cu} is the atomic population on Cu and a_{2M} are the orbital coefficients and φ_{2M} are the five atomic orbitals with $M=-2$ to 2:

$$\phi_{2M}(\vec{r}) = Nr^2 e^{-\zeta r} y_{2M}(\theta,\varphi) \qquad (7)$$

with the normalization condition (one unpaired electron on Cu)

$$\sum_{M=-2}^{2} a_{2M}^2 = 1 \qquad (8)$$

The expression of ρ_{Cu} becomes:

$$\rho_{Cu}(\vec{r}) = p_{Cu}|\sum_{M=-2}^{2} a_{2M} N r^2 e^{-\zeta r} y_{2M}(\theta,\varphi)|^2 \quad (9)$$

Using the properties of the products of Slater functions and the products of real sphericals harmonics,[27] this expression may be written as:

$$\rho_{Cu}(\vec{r}) = p_{Cu}\sum_{l=0}^{l=4}\sum_{m=-l}^{l} P_{lm} N_l R_l(2\zeta,r) y_{lm}(\theta,\varphi) \quad (10)$$

where P_{lm} is a linear combination of products of two orbital coefficients. The analogy between Equations (3) and (10) leads to relationships between the multipole populations and the orbital coefficients, assuming a radial exponent $\zeta = 2\xi$.

No convergence was obtained in the orbital coefficient refinement and therefore refinements were performed applying a constraint on the 3d orbital type for each Cu one after the other. The corresponding agreement factors are reported in Table 3.

Compared with the spherical model, the refinement is improved for Cu1, Cu2, and Cu4 when using an x^2-y^2 or xy constraint. For Cu3, the refinement is slightly improved with an x^2-y^2 or xy constraint and also yz, but deteriorated by others (xz, z^2).

This constrained refinement does not permit to discriminate between x^2-y^2 or xy type for the spin density on Cu. Indeed the same multipoles are involved in both cases (quadrupole z^2 and hexadecapoles z^4 and x^4+y^4) as shown by the expression of the populations in function of the corresponding orbital coefficients a_4 and a_5:

$$P_{20} = -2\frac{5\sqrt{3}}{63} p_{Cu}(a_4^2 + a_5^2) \quad (11)$$

$$P_{40} = \frac{3}{224\pi}\frac{p_{Cu}}{0.069417}(a_4^2 + a_5^2) \quad (12)$$

$$P_{44} = \frac{p_{Cu}}{\pi}(a_4^2 + a_5^2) \quad (13)$$

Based on the theoretical study reported below, the x^2-y^2 type was assumed preferably to xy. Compared to the spherical refinement ($R_w(F_M)=8.47$ and GOF$=2.54$), the refinement is clearly improved by using a constraint with x^2-y^2 orbitals on the four Cu atoms ($R_w(F_M)=8.20$ and GOF$=2.46$). In order to take into account the special case of Cu3 with respect to the other copper atoms as seen in Table 3, a yz component was added to the x^2-y^2 component (with an equal weight) on Cu3 which leads to a slight improvement of the refinement ($R_w(F_M)=8.1$ and GOF$=2.4$). In Table 4 are reported the refined populations corresponding to this last model.

Table 4. Experimental spin populations at 2 K under 6 Tesla in the [Cu_4] cluster (model: The unpaired spin 3d orbital for Cu1, Cu2 and Cu4 is constrained to be of x^2-y^2 type and for Cu3 of ($(x^2-y^2)+yz$) type).

	Spin populations (μ_B)	Spin populations normalized to 4
κ_{Cu} [ua^{-1}]	1.44(8)	
Cu1	0.633(9)	0.738(10)
Cu2	0.608(9)	0.709(10)
Cu3	0.708(9)	0.826(10)
Cu4	0.687(8)	0.801(9)
O1	0.044(10)	0.051(12)
O2	0.115(9)	0.134(10)
O3	0.022(10)	0.026(12)
O4	0.080(9)	0.093(10)
O5	−0.017(10)	−0.020(12)
O6	0.105(11)	0.122(13)
O7	0.094(9)	0.110(10)
O8	0.077(9)	0.090(10)
N1	0.018(11)	0.021(13)
N2	0.089(10)	0.104(12)
N3	0.063(10)	0.073(12)
N4	0.102(9)	0.109(10)
Sum	3.43(4)	4.00
N obs	152	
N param	17	
GOF (=2.43)		
$R_w(F_M)$	0.081	

The Figure 7 displays the section of the spin density in the bridge planes for a symmetrical configuration and a long Cu···Cu distance of 3.3 Å (Figure 7a) and for an asymmetrical configuration and a shorter Cu···Cu distance of 3.1 Å (Figure 7b).

Theoretical calculations: Using the previous Heisenberg Hamiltonian [Eq. (1)] the calculated J values for this cubane complex are $+20.5$ and $+1.85$ cm^{-1}, respectively, for J_1 and J_2 exchange coupling constants (see Section on Computational Details). Such values are in agreement with those found in our previous theoretical study for similar complexes.[12] The difference in strength between both interactions can be easily understood as due to the presence of two long Cu–O bond lengths in the case of the J_2 interaction whilst only one for the J_1 coupling. Hence, for the J_1 interaction the exchange pathway between

Table 3. Refinements with different Cu 3d orbital constraints: agreement factors and goodness of fit.

	Cu1		Cu2		Cu3		Cu4	
	$R_w(F_M)$	GOF	$R_w(F_M)$	GOF	$R_w(F_M)$	χ	$R_w(F_M)$	GOF
x^2-y^2	8.39	2.51	8.35	2.49	8.48	2.53	8.41	2.51
xy	8.39	2.51	8.35	2.49	8.46	2.53	8.42	2.51
xz	8.59	2.56	8.54	2.55	8.57	2.56	8.52	2.55
yz	8.46	2.53	8.55	2.55	8.43	2.52	8.51	2.54
z^2	8.57	2.56	8.61	2.57	8.51	2.54	8.54	2.55

GOF$=[(\Sigma_{hkl}\, w(|F_M^o|-|F_M^c|)^2)/(N_o-N_v)]^{1/2}$ with N_o = number of reflections, N_v = number of parameters and w weighting scheme ($1/\sigma^2$).

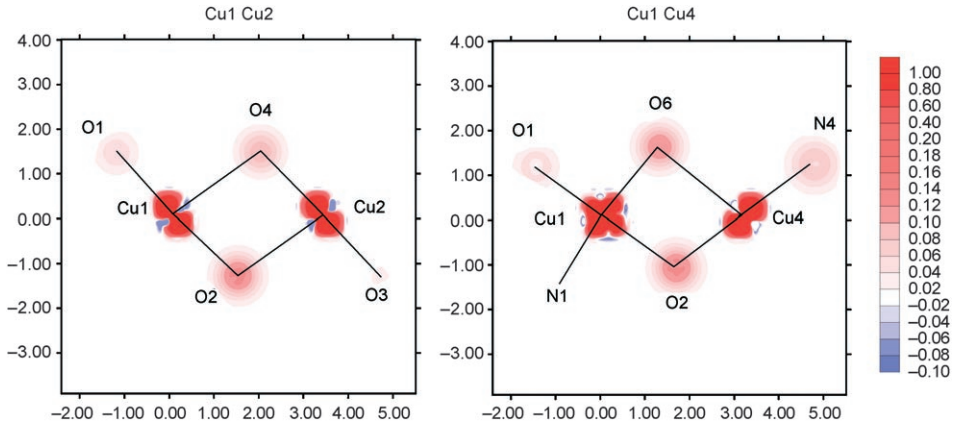

Figure 7. Section of the reconstructed experimental spin density (in $\mu_B/Å^3$) illustrating for the dinuclear planes related to Cu1.

the two copper atoms comprises two short Cu–O bond lengths and consequently results in a stronger exchange interaction. As was previously observed for other similar Cu_4 complexes, the calculated values are different from the fitted ones extracted from the experimental magnetic susceptibility ($J_1 = +30.5\ cm^{-1}$, $J_2 = -5.5\ cm^{-1}$). Indeed, usually the calculated J_2 value corresponds to a weak ferromagnetic (or very weak antiferromagnetic) interaction while the calculated J_1 agrees well with the fitted data but giving a smaller value. In our previous theoretical study,[12] we performed a deep analysis of such discrepancy. We concluded that probably the larger fitted J_1 value could be due to a compensation of the antiferromagnetic J_2 value while the two calculated values are ferromagnetic. Nevertheless, both set of values give a reasonable agreement of the experimental curve (see Figure 4). The curve obtained with the calculated J values is indicated as a dashed line.

A representation of the calculated spin density for the S = 2 ground state can be found in Figure 8. The corresponding atomic spin populations are collected in Table 5. We can outline the predominance of the spin delocalization mechanism due to the presence of the unpaired electrons in the M–L e_g-type antibonding orbitals.[28,29] The spin polarization mechanism only appears to be responsible of very small negative values on some carbon atoms (not detected in Figure 7 due to the employed cut-off value). The predominance of this mechanism on the carbon atoms is nicely represented by the alternation of signs in a sequence of neighboring atoms (see Table 5).

Table 5. Averaged Mulliken, NBO[46] and AIM (Atoms in Molecules)[47] atomic spin populations (see below for labels) using the B3LYP functional for the high spin S = 2 ground state for the studied Cu_4 complex. The spin populations obtained using Polarized Neutron Diffraction are provided for comparison.

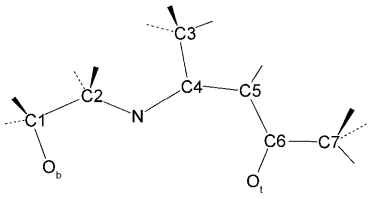

	Mulliken	NBO	PND
Cu	0.624	0.631	0.77(1)
O_b	0.172	0.171	0.11(1)
O_t	0.083	0.086	0.04(1)
N_t	0.111	0.104	0.08(1)
C1	−0.002	−0.001	
C2	0.004	0.002	
C3	0.009	0.008	
C4	−0.016	−0.012	
C5	0.006	0.004	
C6	−0.008	−0.008	
C7	0.008	0.007	

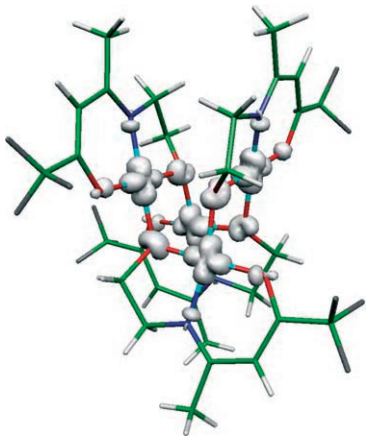

Figure 8. Spin density map, for the S = 2 ground state of the Cu_4 complex, calculated with the B3LYP functional. The isodensity surface represented corresponds to a value of $0.03\ e^-\ bohr^{-3}$ (clear regions indicate positive spin populations, negative values are not detected with the employed cut-off).

Conclusion

In this paper we presented complementary studies on the tetranuclear Cu^{II} complex $[Cu_4L_4]$ with cubane-like structure which we previously reported as a precursor of two series of heterobimetallic copper(II)–lanthanide(III) with four $[LnCu_3]$ and nine $[Ln_3Cu_6]$ nuclearities.[14,15] With the aim to better describe the magnetic properties of this compound, we carried out a spin density study by polarized neutron diffraction, HF-EPR and theoretical calculation. DFT calculations confirm that the predominant ferromagnetic interaction J_1 ($+30.5\ cm^{-1}$) arises from the four Cu–Cu pairs with

the shortest separation while weak antiferromagnetic interactions J_2 ($-5.5\ cm^{-1}$) involve the two pairs with longer separation ($\hat{H} = -\sum_{i>j} 2J_{ij}\hat{S}_i\hat{S}_j$). This is in agreement with the experimental spin density obtained from polarized neutron diffraction study. The spin density is mainly located in the basal plane of the Cu^{II} ions with a distortion of *yz* type for one Cu^{II} ions. Some delocalization is observed on the ligand (L) but to a smaller extent than shown by the DFT calculations. Interestingly, HF-EPR measurements at low temperatures evidence a negative axial Zero-Field Splitting parameter *D* ($-0.25 \pm 0.01\ cm^{-1}$) plus a small rhombic term *E* ($0.025 \pm 0.001\ cm^{-1}$, $E/D = 0.1$).

The results presented here show that such studies allow a good description of the magnetic properties and furthermore they validate the experimental and theoretical tools that will be used in further studies of the more complicated copper(II)–lanthanide(III) systems [$LnCu_3$] and [Ln_3Cu_6]. In this way, they should be understood as a part of a more exhaustive study aimed at understanding the structural parameters driving the magnetic anisotropy in these systems. This is a prerequisite in order to reach a rational approach in the design of single-molecule magnets.

Experimental Section and Computational Methods

Synthesis: The ligand (LH_2) and copper(II) cubane [Cu_4] were synthesized as previously reported.[14,15] Large single crystals used for neutron diffraction were grown by slow evaporation of the reacting solution.

Magnetic measurements: Magnetic measurements were carried out on bulk polycrystalline samples using a PTFE capsule as sample holder with a Quantum Design MPMS SQUID magnetometer. The data were corrected for the diamagnetism of the constituent atoms, using Pascal constants, and of the sample holder.

EPR Study: The HF-EPR spectrometer was operated in transmission configuration (single-pass operation) with oversized brass guides to propagate the exciting frequency from the source (a 95 GHz Gunn oscillator equipped either with a frequency doubler or with a frequency tripler) to the sample and then to the detection (InSb hot-electron bolometer). The main magnetic field is supplied by a superconducting magnet (with 12 T maximum magnetic field) with a small oscillating field superimposed to the main one in order to record the derivative of the transmission. A helium flux cryostat allows working from 1.5 to 300 K. The polycrystalline sample is pressed into a pellet in order to avoid orientation effects due to the large applied magnetic field.

X-ray diffraction structure determination

Data collection: Diffraction data were collected at room temperature by means of the COLLECT program.[30] Lorentz-polarization correction, peak integration and background determination were carried out with the DENZO[31] program. Frame scaling and unit-cell parameters refinement were made through the SCALEPACK program.[31] No absorption correction was applied to the data sets.

Structure solution and refinement: [Cu_4] crystallizes in the monoclinic system. According to the observed systematic extinctions, the structure was solved in the $P2_1/c$ space group by direct methods using the SIR97 programs[32] combined to Fourier difference synthesis and refined against *F* using reflections with [$I > 3\sigma(I)$] using the CRYSTALS program.[33] All thermal atomic displacements for non hydrogen atoms have been refined anisotropically. X-ray crystallographic data and refinement details are summarized in Table 1. Selected interatomic distances and angles are listed in Table S2.

Neutron diffraction structure determination

Data collection: A single crystal of size ($4 \times 3 \times 0.8$) mm^3 was set on the four-circle diffractometer 5C2 of the Laboratoire Léon Brillouin (LLB) and cooled down to 30 K. The data collection details are reported in Table 1. The wavelength was 0.8292 Å. The cell parameters refined at 30 K are: $a = 13.393(3)$, $b = 12.207(3)$, $c = 22.82(14)$ Å, $\beta = 97.224(6)°$. The data collection was performed for theta between 5 and 75°. The integrated intensities of 10677 reflections were measured leading to 1503 unique reflections, allowing the determination of the square of the nuclear structure factors $|F_N(hkl)|^2$ after data reduction. No absorption corrections were performed because of the small value of the linear absorption coefficient, estimated to 2.302 cm^{-1}.

Structure refinement: The atomic parameters determined from X-ray diffraction at 150 K were used as starting parameters for refinement of structure proceeded with the SHELXL97 software.[48] The non-hydrogen atoms of the asymmetric unit atoms were refined anisotropically (full-matrix least squares method on F_N^2). The common isotropic displacement parameter (0.02712 $Å^2$) for hydrogen atoms was refined with a constraint of 1.05 Å for the C–H bonds. The refinement parameters are reported in Table 1.

Polarized neutron diffraction experiment

The classical flipping ratio technique was used to determine the magnetic structure factors which are Fourier components of the magnetization density.[34,35] Two data collections were performed on the 5C1 polarized neutron diffractometer at the LLB for two different orientations of the sample with respect to the vertical applied magnetic field. The wavelength we used was 0.84 Å and the beam polarization equal to 88 per cent. The flipping ratios were measured at 2 K under a high magnetic field of 6 T. First, a large single crystal with a lozenge shape ($5 \times 5 \times 1$) mm^3 was set in the cryomagnet with the *c* direction vertical. A set of 545 flipping ratios $R(hkl)$ was collected with $|h_{max}| = 11$, $|k_{max}| = 9$ and $|l_{max}| = 7$ leading to 184 unique reflections. A second crystal oriented with the *b* axis nearly vertical was used for the second data collection. A set of 392 flipping ratios was then collected with $|h_{max}| = 8$, $|k_{max}| = 6$ and $|l_{max}| = 11$ leading to 126 unique reflections. The nuclear structure factors $F_N(hkl)$ calculated from the neutron structure determined in this work at 30 K were used to derive the experimental magnetic structure factors $F_M(hkl)$ from the flipping ratios. Only the reflections with a large nuclear structure factor ($|F_N| > 1.10^{-12}$ cm) and a flipping ratio $0.5 < R < 2$ were retained for the data analysis. A correction for the nuclear polarization of the hydrogen nuclei by the high external magnetic field at low temperature was applied. The Cu orbital contribution to the magnetic structure factors ion was subtracted from the experimental quantities in order to obtain the structure factors due to spin only. The dipolar approximation[36] was used to estimate this contribution taking a mean value 2.10 for the Landé factor g deduced from the EPR measurements. Two final sets of 184 and 126 magnetic structure factors respectively were obtained including 65 common reflections. The average between the 2 sets of reflections provided a final set of 152 unique reflections with $F_M > 3\sigma(F_M)$.

Computational details

Since a detailed description of the computational strategy used to calculate the exchange coupling constants in polynuclear complexes is outside the scope of this paper, we will only discuss here the most relevant aspects. A detailed description of the methodological approach can be found in the literature.[29,37,38] as well as a review of the results for polynuclear complexes.[39] For a general polynuclear complex, the Heisenberg Hamiltonian without anisotropic terms can be expressed as:

$$\hat{H} = -\sum_{i>j} 2J_{ij}\hat{S}_i\hat{S}_j \qquad (14)$$

where $\hat{S}_i$ and $\hat{S}_j$ are the spin operators of the paramagnetic centers *i* and *j*. The J_{ij} parameters are the exchange coupling constants for the different pairwise interactions between the paramagnetic centers of the molecule. In order to evaluate the *n* different coupling constants J_{ij} present in a polynuclear complex, we need to perform calculations for at least $n+1$ different spin distributions (for the specific case of cubanes, see ref. [8]).

Thus, solving the system of n equations obtained from the energy differences we can obtain the n coupling constants.

Previously, we analyzed the effect of the basis set and the choice of the functional on the accuracy of the determination of the exchange coupling constants.[37,40] The conclusions were that the hybrid B3LYP functional,[41] together with the basis sets proposed by Schaefer et al., provide J values in excellent agreement with the experimental data. We employed a basis set of triple-ζ quality for the transition metal atoms[42] and double-ζ for main group elements.[43] The calculations were performed with the Gaussian 03 code[44] using initial guess functions generated with the Jaguar 6.0 code.[45]

CCDC 604273 contains the supplementary crystallographic data for this paper. These data can be obtained free of charge from The Cambridge Crystallographic Data Centre via www.ccdc.cam.ac.uk/data_request/cif.

Acknowledgements

We thank the "Région Rhône-Alpes" for financial support. Instrumental support for magnetic measurements was provided by the "Commissariat à l'Energie Atomique" (CEA) through a "Laboratoire de Recherche Conventionné" (LRC No DSM-03-31). Y.C. thanks the Marie Curie Incoming International Fellowships (IIF) for financial support through the European Community's Sixth Framework Programme. The research reported by J.T. and E.R. was supported by the Dirección General de Investigación del Ministerio de Educación y Ciencia and Comissió Interdepartamental de Ciència i Tecnologia (CIRIT) through grants CTQ2005-08123-C02-02/BQU and 2005SGR-00036, respectively. The computing resources were generously made available at the Centre de Computació de Catalunya (CESCA) through a grant provided by Fundació Catalana per a la Recerca (FCR) and the Universitat de Barcelona.

[1] J. A. Bertrand, A. P. Ginsberg, R. I. Kaplan, C. E. Kirkwood, R. L. Martin, C. Sherwood, *Inorg. Chem.* **1971**, *10*, 240–246.
[2] L. Merz, W. Haase, *Z. Naturforsch.* **1976**, *31a*, 177–182.
[3] W. J. Jones, S. Gupta, L. J. Theriot, F. T. Helm, W. A. Baker Jr., *Inorg. Chem.* **1978**, *17*, 87–90.
[4] K. Dimitrou, K. Folting, W. E. Streib, G. Christou, *J. Am. Chem. Soc.* **1993**, *115*, 6432–6433.
[5] M. A. Halcrow, J.-S. Sun, J. C. Huffman, G. Christou, *Inorg. Chem.* **1995**, *34*, 4167–4177.
[6] S. M. J. Aubin, M. W. Wemple, D. M. Adams, H.-L. Tsai, G. Christou, D. N. Hendrickson, *J. Am. Chem. Soc.* **1996**, *118*, 7746–7754.
[7] H. Oshio, N. Hoshino, T. Ito, *J. Am. Chem. Soc.* **2000**, *122*, 12602–12603.
[8] E. Ruiz, A. Rodríguez-Fortea, P. Alemany, S. Alvarez, *Polyhedron* **2001**, *20*, 1323.
[9] E.-C. Yang, W. Wernsdorfer, S. Hill, R. S. Edwards, M. Nakano, S. Maccagnano, L. N. Zakharov, A. L. Rheingold, G. Christou, D. N. Hendrickson, *Polyhedron* **2003**, *22*, 1727–1733.
[10] H. Oshio, N. Hoshino, T. Ito, M. Nakano, *J. Am. Chem. Soc.* **2004**, *126*, 8805–8812.
[11] H. Oshio, M. Nihei, S. Koizumi, T. Shiga, H. Nojiri, M. Nakano, N. Shirakawa, M. Akatsu, *J. Am. Chem. Soc.* **2005**, *127*, 4568–4569.
[12] J. Tercero, E. Ruiz, S. Alvarez, A. Rodríguez-Fortea, P. Alemany, *J. Mater. Chem.* **2006**, *16*, 2729.
[13] E.-C. Yang, W. Wernsdorfer, L. N. Zakharov, Y. Karaki, A. Yamaguchi, R. M. Isidro, G.-D. Lu, S. A. Wilson, A. L. Rheingold, H. Ishimoto, D. N. Hendrickson, *Inorg. Chem.* **2006**, *45*, 529–546.
[14] C. Aronica, G. Chastanet, G. Pilet, B. Le Guennic, V. Robert, W. Wernsdorfer, D. Luneau, *Inorg. Chem.* **2007**, *46*, 6108–6119.
[15] C. Aronica, G. Pilet, G. Chastanet, W. Wernsdorfer, J.-F. Jacquot, D. Luneau, *Angew. Chem.* **2006**, *118*, 4775–4778; *Angew. Chem. Int. Ed.* **2006**, *45*, 4659–4662.
[16] J. Tang, I. Hewitt, N. T. Madhu, G. Chastanet, W. Wernsdorfer, C. E. Anson, C. Benelli, R. Sessoli, A. K. Powell, *Angew. Chem.* **2006**, *118*, 1761–1765; *Angew. Chem. Int. Ed.* **2006**, *45*, 1729–1733.
[17] A. L. Barra, L. C. Brunel, D. Gatteschi, L. Pardi, R. Sessoli, *Acc. Chem. Res.* **1998**, *31*, 460–466.
[18] C. Aronica, E. Jeanneau, H. El Moll, D. Luneau, B. Gillon, A. Goujon, A. Cousson, M. A. Carvajal, V. Robert, *Chem. Eur. J.* **2007**, *13*, 3666–3674.
[19] M. Bonnet, D. Luneau, E. Ressouche, P. Rey, J. Schweizer, M. Wan, H. Wang, A. Zheludev, *Mol. Cryst. Liq. Cryst.* **1995**, *271*, 35–53.
[20] D. Bordeaux, J. X. Boucherle, B. Delley, B. Gillon, E. Ressouche, J. Schweizer, *Z. Naturforsch. A: Phys. Sci.* **1993**, *48*, 117–119.
[21] R. Caciuffo, O. Francescangeli, L. Greci, S. Melone, B. Gillon, G. Amoretti, *Physica B+C* **1992**, *180–181*, 76–78.
[22] E. Ressouche, J. X. Boucherle, B. Gillon, P. Rey, J. Schweizer, *J. Am. Chem. Soc.* **1993**, *115*, 3610–3617.
[23] A. Zheludev, M. Bonnet, D. Luneau, E. Ressouche, P. Rey, J. Schweizer, *Physica B+C* **1995**, *213–214*, 268–271.
[24] A. Bencini, D. Gatteschi in *EPR of exchange coupled systems*, Springer, Berlin, **1990**.
[25] P. J. Brown, A. Capiomont, B. Gillon, J. Schweizer, *Mol. Phys.* **1983**, *48*, 753–761.
[26] E. Clementi, D. L. Raimondi, *J. Chem. Phys.* **1963**, *38*, 2686.
[27] A. Holladay, P. Leung, P. Coppens, *Acta Crystallogr. Sect. A* **1983**, *39*, 377.
[28] E. Ruiz, J. Cirera, S. Alvarez, *Coord. Chem. Rev.* **2005**, *249*, 2649.
[29] J. Cano, E. Ruiz, S. Alvarez, M. Verdaguer, *Comments Inorg. Chem.* **1998**, *20*, 27.
[30] Nonius, *COLLECT*, Nonius B. V., Delft, The Netherlands, **1997–2001**.
[31] Z. Otwinowski, W. Minor, *Methods in Enzymology*, Academic Press, New York, **1997**.
[32] A. Altomare, M. C. Burla, M. Camalli, G. L. Cascarano, C. Giacovazzo, A. Guagliardi, A. G. G. Moliterni, G. Polidori, R. Spagna, *J. Appl. Cryst.* **1999**, *32*, 115–119.
[33] D. J. Watkin, C. K. Prout, J. R. Carruthers, P. W. Betteridge, *CRISTAL Issue 11*, Chemical Crystallography Laboratory, Oxford, UK, **1999**.
[34] J. B. Forsyth in *Electron and Magnetization densities in Molecules and Crystals*, NATO Advanced Study Institutes Series, Series B: Physics, *Vol. 48* (Ed.: P. Becker), Plenum Press, New York, **1980**.
[35] B. Gillon, C. Mathonière, E. Ruiz, S. Alvarez, A. Cousson, T. Rajendiran, O. Kahn, *J. Am. Chem. Soc.* **2002**, *124*, 14433–14441.
[36] G. L. Squires in *Introduction to the theory of thermal neutron scattering*, University Press, Cambridge, **1978**, p. 139.
[37] E. Ruiz, S. Alvarez, J. Cano, V. Polo, *J. Chem. Phys.* **2005**, *123*, 164110(1)–164100(7).
[38] E. Ruiz, A. Rodríguez-Fortea, J. Cano, S. Alvarez, P. Alemany, *J. Comput. Chem.* **2003**, *24*, 982–989.
[39] E. Ruiz, *Struct. Bonding (Berlin)* **2004**, *113*, 71–102.
[40] E. Ruiz, S. Alvarez, A. Rodríguez-Fortea, P. Alemany, Y. Pouillon, C. Massobrio in *Magnetism: Molecules to Materials, Vol. 2* (Eds.: J. S. Miller, M. Drillon), Wiley-VCH, Weinheim, **2001**, p. 227.
[41] A. D. Becke, *J. Chem. Phys.* **1993**, *98*, 5648–5652.
[42] A. Schaefer, C. Huber, R. Ahlrichs, *J. Chem. Phys.* **1994**, *100*, 5829–5835.
[43] A. Schaefer, H. Horn, R. Ahlrichs, *J. Chem. Phys.* **1992**, *97*, 2571–2577.
[44] Gaussian 03 (Revision C1), M. J. Frisch, G. W. Trucks, H. B. Schlegel, G. E. Scuseria, M. A. Robb, J. R. Cheeseman, J. A. Montgomery, T. Vreven, K. N. Kudin, J. C. Burant, J. M. Millam, S. S. Iyengar, J. Tomasi, V. Barone, B. Mennucci, M. Cossi, G. Scalmani, N. Rega, G. A. Petersson, H. Nakatsuji, M. Hada, M. Ehara, K. Toyota, R. Fukuda, J. Hasegawa, H. Ishida, T. Nakajima, Y. Honda, O. Kitao, H. Nakai, M. Klene, X. Li, J. E. Knox, H. P. Hratchian, J. B. Cross, C. Adamo, J. Jaramillo, R. Gomperts, R. E. Stratmann, O. Yazyev, A. J. Austin, R. Cammi, C. Pomelli, J. Ochterski, P. Y. Ayala, K. Morokuma, G. A. Voth, P. Salvador, J. J. Dannenberg, V. G. Zakrzewski, S. Dapprich, A. D. Daniels, M. C. Strain, O. Farkas, D. K. Malick, A. D. Rabuck, K. Raghavachari, J. B. Foresman, J. V. Ortiz, Q. Cui, A. G. Baboul, S. Clifford, J. Cioslowski, B. B. Stefanov, G. Liu, A. Liashenko, P. Piskorz, I. Komaromi, R. L. Martin, D. J. Fox,

T. Keith, M. A. Al-Laham, C. Y. Peng, A. Nanayakkara, M. Challacombe, P. M. W. Gill, B. Johnson, W. Chen, M. W. Wong, C. Gonzalez, J. A. Pople, Gaussian, Inc., Pittsburgh, PA, **2003**.
[45] *Jaguar 6.0*, Schrödinger, Inc., Portland, **2005**.
[46] A. E. Reed, L. A. Curtiss, F. Weinhold, *Chem. Rev.* **1988**, *88*, 899–926.
[47] R. F. W. Bader, *Atoms in Molecules A: Quantum Theory*, Oxford University Press, Oxford, **1994**.
[48] G. M. Sheldrick, *Acta Crystallogr. Section A* **2008**, *64*, 112–122.

Received: March 26, 2008
Published online: September 12, 2008

